Stress-induced multiple quantum phase transitions in the *B*1 and *B*2 phases of CeN

Min Liu [1,*] and Yuanji Xu [2]

[1]*College of Mathematics and Physics, Beijing University of Chemical Technology, Beijing 100029, China*
[2]*Institute for Applied Physics, University of Science and Technology Beijing, Beijing 100083, China*

The quantum phase transition in Ce-based compounds has attracted significant attention in strongly correlated systems, primarily due to the dual nature of f electrons. Rare-earth nitride (Re-N) compounds are particularly intriguing, as they exhibit major physical mechanisms such as the Kondo effect or mixed-valence behavior. Notably, CeN is anomalously small in lattice parameter compared with other Re-N compounds and there is a structure phase transition from B1-type (NaCl-type) to B2-type (CsCl-type) at approximately 77 GPa. Hence, we study the electronic structures of B1-type and B2-type CeN by tuning stress, employing the DFT+DMFT method. Our results clarify the B1-type CeN is in a mixed-valence state at ambient pressure. However, as the system experiences compression and tension, CeN undergoes multiple quantum phase transitions, transitioning from a mixed-valence state to a Kondo metal and ultimately to an insulator. Importantly, it is observed that the number of occupied $4f$ electrons n_f of Ce increases as the temperature and pressure increase within the mixed-valence regime, contrasting with the behavior observed in the Kondo regime, the n_f is very stable, nearly one. Furthermore, we also investigate the high-pressure phase of B2-type CeN, it also presents mixed-valence and Kondo metal phases transition by tuning stress. Our paper illustrates stress as a clean method to tune quantum phase transitions in CeN by changing the states of f electrons and clarifying the physical driving force of phase transitions.

I. INTRODUCTION

The rare-earth compounds exhibit abundant novel phenomena, such as heavy fermion behavior, quantum phase transition, unconventional superconductivity, due to their strong electron correlated effect and dual nature of f electrons [1–4]. The rare-earth nitrides (Re-N) are a unique family of materials characterized by a rock-salt crystal structure. These materials possess distinctive magnetic, electronic, and optical properties due to their partially occupied and remarkably localized $4f$ electrons. They can exhibit a wide range of behaviors, including being metallic, semimetallic, half-metallic, semiconducting, or insulating [5–15]. The rare-earth nitrides have various fascinating applications, such as in spintronics [16–20], infrared (IR) detectors [21,22], contactors [21], catalysts [23], and magnetic refrigeration [24,25]. More intriguingly, they display exotic properties like superconductivity [19,20] and the Kondo effect [26], as well as mixed-valence phenomena [27–30]. Notably, the Kondo effect and the mixed-valence physics in strongly correlated $4f$-electron systems have been the subject of longstanding controversy, and both phenomena are found in CeN, which makes CeN an ideal material platform to explore the interplay of these two phenomena [27–30].

Among the various systems in the Re-N family, CeN is particularly interesting. Despite being studied for several decades, there are still some debated issues surrounding it.

At ambient pressure, CeN forms a face-centered-cubic (fcc) structure of rock-salt B1-type. The lattice parameter of CeN is anomalously small compared to LnN (Ln = La, Pr, Nd, Sm, Eu, and others) and CeX (X = P, As, Sb, Bi, and others), indicating a 4^+ Ce configuration in CeN, while the other rare-earth nitrides have a 3^+ valence [11,31]. This suggests that CeN shares similarities with the collapsed α phase of cerium metal, in which the cerium $4f$ electrons are itinerant and play a crucial role in metallic conduction and coherent properties. In contrast, other CeX compounds are more similar to the γ phase of cerium metal, in which the cerium $4f$ electrons are localized [32]. However, high-energy spectroscopy experiments (XPS and BIS) have found that the effective valence of cerium in B1-type CeN is close to 3^+ [33]. Optical conductivity data, on the other hand, suggests a slightly higher effective valence of 3.48^+ [34]. Additionally, the effective valence obtained from the lattice constant is approximately 3.85^+ at room temperature but approaches 3^+ as the temperature rises to 1100 K [29].

CeN was considered a classic example of a mixed-valence compound, where the localized $4f$ electrons weakly hybridize with the conduction electrons [27–30]. This results in a ground state composed of a mixture of $4f^0$ and $4f^1$ ions, which is a homogeneous mixed valence [35]. The distinctive behavior of the $4f$ electron in the Ce ion leads to CeN exhibiting numerous anomalous properties, including anomalous lattice parameters, elastic constants, compressibility, thermal expansion coefficients, and magnetic susceptibility, among others [36]. However, some researchers have emphasized that the two valence configurations (tetravalent $4f^0$ and trivalent

*minliu@buct.edu.cn

$4f^1$) are not degenerate, making mixed valence in the ground state of CeN highly unlikely [37]. They argue that the $4f$ electron in CeN has mainly an itinerant character.

There are also other controversial points. For example, Sclar proposed that CeN is a semiconductor with a band gap of 1.8 eV [10]. Xiao *et al.* also indicated that CeN is a *p*-type semiconductor with an optical band gap of 1.76 eV [38]. On the other hand, Lee *et al.* reported that CeN is a metal based on x-ray diffraction (XRD) and transmission electron microscopy [39]. The controversies surrounding the electronic structure of CeN have led to further analysis in this paper. Recently, an XRD experiment observed that at high pressure, the *B*1-type CeN (Fm-3m) transforms to the *B*2-type CeN (Pm-3m) at approximately 77 GPa [40]. However, the electronic structure of *B*2-type CeN is only known from DFT results, and there is limited research on the behavior of the $4f$ electron in *B*2-type CeN.

To address the controversies regarding the effective valence of Ce ions in CeN and its electronic properties, in this paper, we investigate the occupied electrons of Ce-$4f (n_f)$, spectral function, renormalization factor Z, Fermi surface, and the imaginary part of the real frequency self-energy employing the DFT+DMFT method. First, we found that the *B*1-type CeN exhibits a metallic behavior at ambient pressure. By varying the temperature of *B*1-type CeN from 30 to 1000 K, we found that Ce $-4f$ electrons present a mixed-valence state, supported by spectral function, renormalization factor Z, and Fermi surface analyses. Second, we tuned the global stress by compressing or extending the lattice of *B*1-type CeN. Stress was found to induce multiquantum phase transitions, transforming from mixed-valence to Kondo metal, and then to insulator from compression to tension. Specifically, when the lattice size is smaller than 5.1 Å, the mixed-valence state, having localized $4f$ electrons, is observed with weak $c-f$ electron hybridization near the Fermi level. Importantly, it is observed that the number of occupied $4f$ electrons n_f of Ce increases as the temperature and pressure increase within the mixed-valence regime. When the lattice size is between 5.1 and 5.6 Å, CeN becomes a Kondo metal with strong $c-f$ electrons hybridization and the n_f of Ce is nearly one. However, when the lattice size exceeds 5.6 Å, an insulator state is observed. This suggests a localization to itineration transition of $4f$ electrons in CeN under stress. We further conducted electronic structure calculations on the *B*2-type CeN and found it also exhibits a mixed-valence to Kondo metal quantum phase transitions by tuning stresses. Our paper illustrates stress as a clean method to tune quantum phase transitions in CeN by changing the states of f electrons and clarifying the physical driving force of phase transitions.

II. METHODS

We obtain DFT electronic structures of *B*1-type and *B*2-type CeN based on the full-potential augmented plane-wave method with the generalized gradient approximation (GGA) exchange-correlation functional by Perdew, Burke, and Ernzerhof [41], as implemented in the WIEN2k code [42]. The Muffin-tin radii are 2.50 a.u. and 2.20 a.u. for Ce, N, respectively. The maximum modulus for the reciprocal vector Kmax was chosen such that RMT*Kmax = 8.0. All

calculations were converged on a grid of 5000 k points in the Brillouin zone. And for *B*1-type and *B*2-type CeN, the structural relaxations were carried out using VASP [43,44]. For VASP calculations, the cutoff energy of 600 eV is chosen with the exchange-correlation functional of GGA-PBE. The projected augmented wave is adopted as the pseudopotentials [45]. The lattice constants and internal coordinates are optimized until the atomic forces become less than 10^{-4} eV/Å. We performed fully charge self-consistent DFT+DMFT calculations to treat the electronic correlations of Ce $-4f$ orbitals using the eDMFT package [46], which is based on the full-potential linear augmented plane-wave method implemented in the WIEN2k code. The hybridization expansion continuous-time quantum Monte Carlo (CT-HYB) was used as the impurity solver [47] and the exact scheme for double counting [48]. Ce-$4f$ local orbitals were constructed using projectors with an energy window from –10 to 10 eV relative to the Fermi energy. The Coulomb interaction was chosen to be $U = 5.5$ eV and $J_H = 0.68$ eV [49]. And all the calculations are performed considering the SOC effect. The self-energy in real frequency was obtained by analytic continuation based on the maximum entropy [50,51].

III. RESULTS AND DISCUSSION

A. The electronic structures of *B*1-type CeN at ambient pressure

At ambient pressure, *B*1-type CeN crystallizes in the rock-salt crystal structure. Its room-temperature lattice constant is 5.02 Å, which is anomalously small compared with other rare-earth mononitrides [29,31]. The Ce–Ce distance of CeN is 3.57 Å, which lies just between those of γ-Ce (3.65 Å) and α-Ce (3.43 Å) [52]. Each Ce atom is surrounded by six nearest neighbors of N at a distance of 2.52 Å. The relaxed lattice parameter is 5.022 Å, very close to the experimental value of 5.02 Å. Therefore, all the calculations presented in this paper have been carried out using the experimental lattice parameter. We first computed the DFT band structures both without and with the spin-orbit coupling effect (SOC), as depicted in Fig. S1 within the Supplemental Material (SM) [53]. These results suggest that Ce $-4f$ electrons predominantly reside near the Fermi level. Additionally, there is a slight hybridization between Ce $-4f$ electrons and Ce-d electrons within the energy range –1.4 to –0.5 eV. Below –2 eV, the characteristic electronic structure primarily exhibits N-p electrons. Upon including SOC, we observe the splitting of Ce-$4f_{5/2}$ and Ce-$4f_{7/2}$ orbitals, as illustrated in the density of states (DOS) plot in Fig. S2 within the SM [53]. This modification leads to the opening of a gap at approximately 0.3 eV, as well as the appearance of two Dirac cones within the gap. It is noteworthy that the Ce $-4f$ orbital exhibits a narrow, flat band with a limited bandwidth, indicating strong electron correlation. To gain further insights into the electronic structures, we employed DFT+DMFT for our analysis.

We systematically investigated the electronic structures of CeN at various temperatures, in the range 30–1000 K. In Fig. 1(a), we present the momentum-resolved spectral function of *B*1-type CeN at 30 K. Notably, the Ce $-4f$ orbital has been significantly shifted closer to the Fermi level compared with the DFT result. This shift indicates a pronounced electron
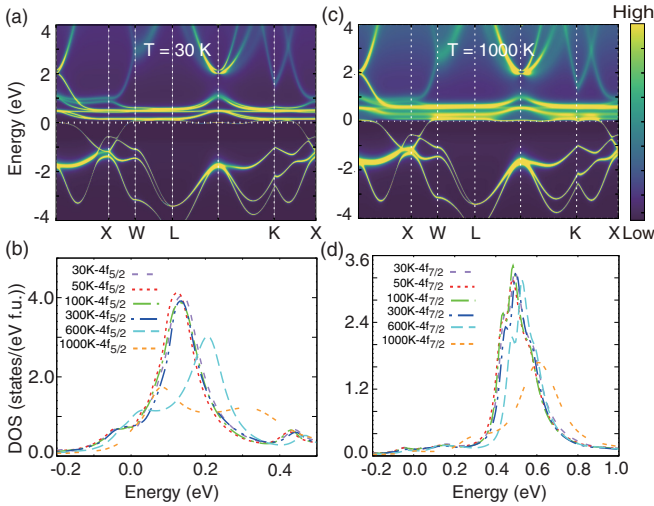
FIG. 1. The electronic structures of B1-type CeN at ambient pressure using DFT+DMFT method. (a) The momentum-resolved spectral function of CeN at 30 K. (b) The spectral density of Ce-4$f_{5/2}$ orbitals from 30 to 1000 K. (c) The momentum-resolved spectral function of CeN at 1000 K. (d) The spectral density of Ce-4$f_{7/2}$ orbitals from 30 to 1000 K.

FIG. 2. The number of the occupied $4f$ electrons n_f, renormalization factor Z and Fermi surface. (a) The number of occupied f electrons n_f of B1-type CeN as a function of temperature from 10 to 1000 K. (b) The renormalization factor Z of Ce-4$f_{5/2}$ and Ce-4$f_{7/2}$ at different temperatures. (c) The Fermi surface at 30, 300, 600, and 1000 K, respectively.

renormalization effect within the Ce $-$ $4f$ bands at lower temperatures. However, at the high temperature 1000 K as shown in Fig. 1(c), it can be seen that the weight of spectral function is much smaller than that of low temperature, which means Ce $-$ $4f$ electrons exhibit localized behavior with weak c–f hybridization at high temperature. Hence, we propose that B1-type CeN has a strong $4f$ electron renormalization effect, which can also shown in the spectral density of Ce-4$f_{5/2}$ and Ce-4$f_{7/2}$ as shown in Figs. 1(b) and 1(d). The Ce-4$f_{5/2}$ and Ce-4$f_{7/2}$ orbitals clearly exhibit splitting due to the influence of SOC, in agreement with the DFT results. Interestingly, the height of the Ce-4$f_{5/2}$ peak decreases notably as the temperature rises, particularly evident at 600 K. However, it experiences relatively minor changes within the temperature range 30–300 K, implying that Kondo behavior may not be prominently exhibited. This trend is similarly observed in the spectral density of the Ce-4$f_{7/2}$ orbital.

To further investigate the electron renormalization effect of B1-type CeN, as illustrated in Fig. 2(a), we initially examined the number of occupied $4f$ electrons n_f of B1-type CeN as a function of temperature from 10 to 1000 K, respectively. It can be seen that the n_f monotonically increases as the temperature increases, which is in agreement with the experiment that at the high temperature the valence of Ce ion is trivalent $4f^1$ [29]. To quantify the electronic correlation effects of the Ce $-$ $4f$ orbital, we also investigated the renormalization factor $Z=m_{DFT}/m^*$ of Ce-4$f_{5/2}$ and Ce-4$f_{7/2}$ at different temperatures as shown in Fig. 2(b). Z is also called the quasiparticle weight $Z = 1/(1 - \frac{\partial \, \mathrm{Im} \, \Sigma(i\omega_n)}{\partial \omega_n}|_{\omega_n \to 0})$, which is a straightforward and quantitative way to characterize the strength of electronic correlations. To minimize numerical errors, specifically those arising from analytic continuation based on the maximum entropy of the real frequency self-energy, we utilized the imaginary part of the Matsubara
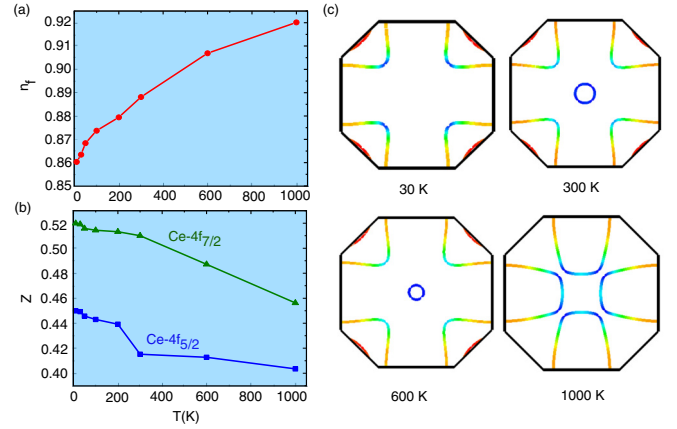
self-energy. The determination of Z involved fitting a fourth-order polynomial to the lowest six points of the Matsubara self-energy and extrapolating. The results reveal a decrease in Z for Ce-4$f_{5/2}$ and Ce-4$f_{7/2}$ with increasing temperature, implying that at high temperatures, the effective mass m^* of Ce-4$f_{5/2}$ and Ce-4$f_{7/2}$ is significantly larger than that at lower temperatures. This trend is contrary to the expectations of Kondo physics and aligns with the analysis of the Ce-4$f_{5/2}$ spectral density. Furthermore, it indicates that B1-type CeN consists of a mixture of $4f^0$ and $4f^1$ ions, resulting in a homogeneous mixed-valence state. The localized $4f$ electrons weakly hybridize with the conduction electrons, with the renormalization effect being more pronounced for Ce-4$f_{5/2}$ due to the presence of occupied $4f$ electrons. Additionally, we also analyzed the Fermi surface at 30, 300, 600, and 1000 K, as displayed in Fig. 2(c). It becomes apparent that the Fermi surface pattern undergoes a Lifshitz transition from low to high temperatures, indicating the strong renormalization effect of Ce $-$ $4f$ electrons.

B. Stress-induced multi-quantum phase transitions in B1-type CeN

We investigated the electronic structures at ambient pressure, but there are few results of electronic structures by compression and tension lattice. Therefore, we decided to explore how stress impacts the electronic structures. We systematically tuned the electronic structures by varying lattice parameters, ranging from the smallest lattice at 4.2 Å to the largest tension lattice at 5.9 Å. Remarkably, our investigation revealed the presence of three distinct phase transitions, each associated with notable changes in the electronic structure, as illustrated in Fig. 3. We present the electronic structures of these three phases from $a = 4.5, 5.2$ to 5.8 Å. At $a = 4.5$ Å, the spectral function demonstrates metallic behavior, as depicted in Fig. 3(a). Notably, the electronic structures remain largely unchanged across the temperature range 50–1000 K. This is because both the Ce-4$f_{5/2}$ and Ce-4$f_{7/2}$ orbitals are
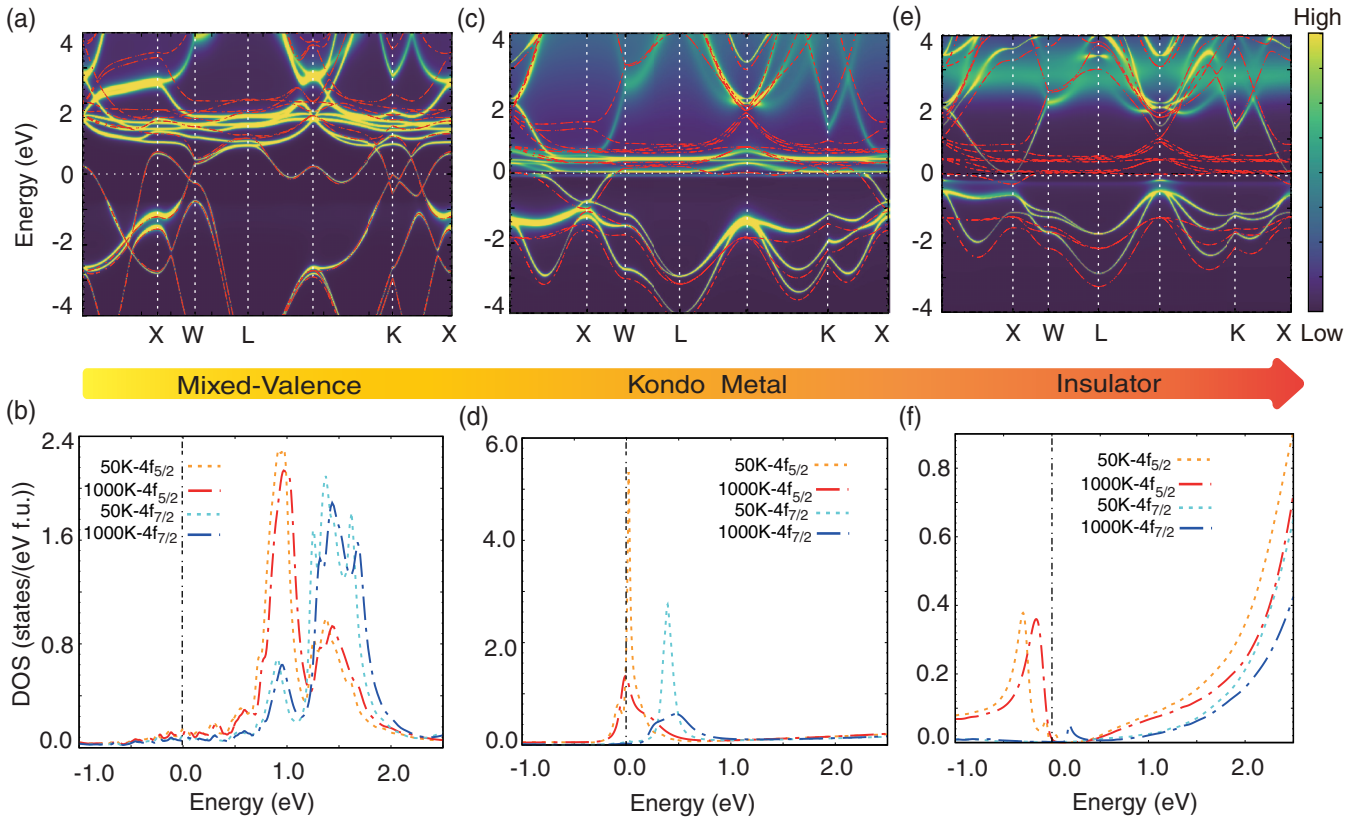
FIG. 3. The momentum-resolved spectral function and spectral density of $B1$-type CeN at different quantum states. [(a),(b)] In the mixed-valence state, the spectral function of CeN, when a equals 4.5 Å at 50 K. The spectral density of Ce-$4f_{5/2}$ and Ce-$4f_{7/2}$ at 50 and 1000 K. [(c),(d)] In the Kondo metal state, the spectral function of CeN, when a equals 5.2 Å at 50 K. The spectral density of Ce-$4f_{5/2}$ and Ce-$4f_{7/2}$ at 50 and 1000 K. [(e),(f)] In the insulator state, the spectral function of CeN, when a equals 5.8 Å at 50 K. The spectral density of Ce-$4f_{5/2}$ and Ce-$4f_{7/2}$ at 50 and 1000 K.

located far from the Fermi level as shown in Fig. 3(b). The red line represents the DFT band, and it closely aligns with the DMFT band near the Fermi level, which means at $a = 4.5$ Å, the Ce $-4f$ localized electrons exhibit weak $c-f$ electrons hybridization showing a mixed-valence state. But when $a = 5.2$ Å, compared with the DFT band, it can be seen that there exist flat bands located at the Fermi level as shown in Fig. 3(c). And at the low temperature T = 50 K, we can see a sharp peak of Ce-$4f_{5/2}$ orbital emerges at the Fermi level. In contrast, at a high temperature of T = 1000 K, as shown in Fig. 3(d), the Ce-$4f_{5/2}$ orbital no longer exhibits the sharp peak. This observation signifies that at low temperatures, there is a strong $c-f$ electrons hybridization, indicating a strong Kondo resonance peak. But when a = 5.8 Å, the DFT band shows metal, the DMFT band suggests insulating behavior, as illustrated in Figs. 3(e) and 3(f), and the spectral density of Ce-$4f_{5/2}$ and Ce-$4f_{7/2}$ orbitals open a gap of 0.18 eV.

To provide a comprehensive view of the three quantum phase transitions, we investigated the number of occupied $4f$ electrons n_f and the renormalization factor Z for Ce-$4f_{5/2}$ and Ce-$4f_{7/2}$ as a function of lattice parameter a under various compression and tension stresses, as depicted in Figs. 4(a) and 4(b). Our findings reveal several intriguing insights. When a is less than 5.1 Å, the system is in a mixed-valence state, as the Ce $-4f$ electrons are pushed a little far away the Fermi level. Importantly, this regime does not exhibit the Kondo

effect. This observation is further supported by the derivative $d(n_f)/d(V/V_0)$, which displays an inflection point, as demonstrated in Fig. 4(a). It means from 4.2 to 5.02 Å ($V/V_0 = 0.59$ to 1.0), the system consistently maintains the mixed-valence state, corroborating our earlier analysis of the renormalization factor Z for Ce-$4f_{5/2}$ and Fermi surfaces at $a = 5.02$ Å as presented in Fig. 2. Examining the number of occupied $4f$ electrons n_f, we note that when we subject the crystal to greater compression, the valence of Ce approaches nearly 4^+. Within the mixed-valence state, n_f displays a quadratic parabolic behavior. However, when the lattice parameter falls
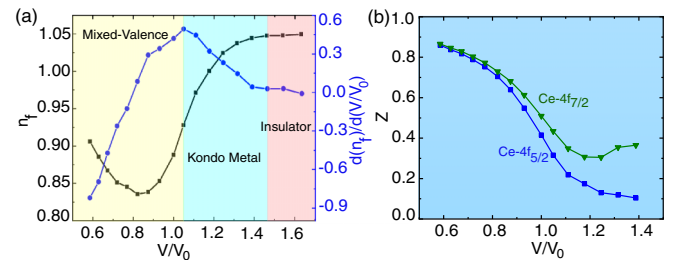

FIG. 4. The multi-quantum phase transitions. (a) The number of occupied $4f$ electrons n_f and derivative $d(n_f)/d(V/V_0)$. (b) The renormalization factor Z of Ce-$4f_{5/2}$ and Ce-$4f_{7/2}$ based on the volume of $B1$-type CeN at different compression and tension stresses.
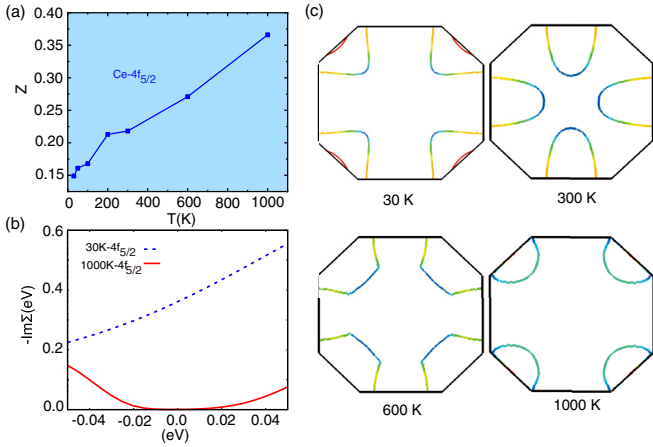
FIG. 5. The Kondo state when a equals 5.2 Å. (a) The renormalization factor Z of Ce-$4f_{5/2}$ of $B1$-type CeN as a function of temperature from 10 to 1000 K. (b) The imaginary part of real frequency self-energy of Ce-$4f_{5/2}$ and Ce-$4f_{7/2}$ at 30 and 1000 K, respectively. (c) The Fermi surface at 30, 300, 600, and 1000 K, respectively.

within the range 5.1–5.6 Å, the system assumes a Kondo metal state. To illustrate, consider the case at a lattice parameter of 5.2 Å, the renormalization factor Z of Ce-$4f_{5/2}$ increases monotonically with rising temperature. In addition, we find the n_f is nearly one, which is very stable with temperature and stress conditions. This behavior contradicts the mixed-valence state, as shown in Fig. 5(a), signifying strong $c-f$ electrons hybridization. Note that due to the limitation of our DMFT calculations, the low T instability of the Kondo metal state is not studied in this paper [54]. Further insights are gained from our investigation into the imaginary part of the real frequency self-energy at both 30 K and 1000 K, presented in Fig. 5(b). These findings reveal disparate behaviors at the low and high temperatures, underscoring the presence of the Kondo effect. Additionally, our analysis of the Fermi surface at 30, 300, 600, and 1000 K, as shown in Fig. 5(c), demonstrates that at a low temperature, a large Fermi surface is observed, but at a high temperature, a small Fermi surface emerges, indicating a typical $c-f$ hybridization and strong Kondo effect. However, when the lattice parameter falls within the range 5.7–5.9 Å, the system exhibits insulating behavior. This behavior can be readily explained by the application of pressure, which reduces the lattice constant, thereby increasing the width of the band and inducing a transition from insulator to metal. This is a common physical phenomenon in solid materials known as the Wilson transition, which refers to the high pressure-induced transition from insulator to metal. On the contrary, extending the lattice constant reduces the width of the band, triggering a transition from metal to insulator.

C. Stress-induced multi-quantum phase transitions in $B2$-type CeN

In the experiment, the $B1$-type CeN transferred to the $B2$-type at about 77 GPa [40]. Hence, it is essential to study the $B2$-type CeN, especially for the Ce $-4f$ electrons behavior. $B2$-type CeN crystallizes in the body-centered cubic
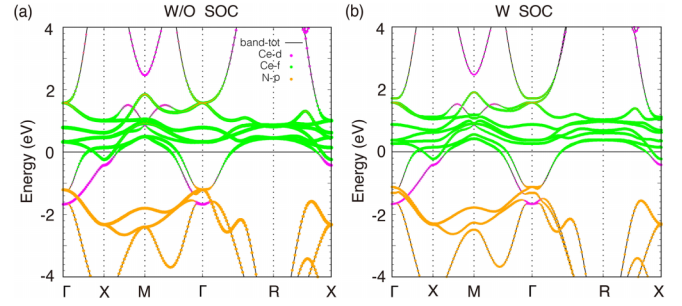

FIG. 6. The DFT band of $B2$-type CeN. (a) without SOC effect, (b) with SOC effect.

crystal structure with the space group of Pm-3m. We obtain the lattice a is 3.029 Å, after the structure relaxation. The Ce–Ce distance in CeN also is 3.029 Å, which is much smaller than that of $B1$-type CeN (3.57 Å). Furthermore, it is considerably shorter than the Ce–Ce distances in γ-Ce (3.65 Å) and α-Ce (3.43 Å). Each Ce atom is surrounded by eight nearest neighbors of N atom at a distance of 2.62 Å. We did the DFT band structure without and with SOC effect as presented in Fig. 6. It is evident that Ce $-4f$ electrons are predominantly located near the Fermi level. These Ce $-4f$ electrons exhibit strong hybridization with Ce-d electrons in proximity to the Fermi level, as well as with N-p electrons in the energy range -2 to -1 eV as depicted in Fig. 6(a). When considering the SOC effect, it shows the bands at M, Γ, and R points break the symmetry making degenerate bands split into two-fold and fourfold degenerate bands, which can form symmetry-enforced semimetal with degeneracy at the Fermi level as shown in Fig. 6(b). Further exploration of correlated topological properties is planned for future work. To investigate the correlated Ce $-4f$ electrons behavior of $B2$-type CeN, we also did DFT+DMFT calculations to comprehensively investigate the electronic structure of the system.

To explore how stress influences the quantum phase transitions in $B2$-type CeN, we systematically modulated the electronic structures through lattice compression and tension. Specifically, we examined the electronic structure at lattice parameters a equal to 2.50, 3.029, and 3.50 Å. Our investigation covered a temperature range 30–1000 K, utilizing the DFT+DMFT method, which includes the consideration of SOC effect. As depicted in Fig. 7, $B2$-type CeN exhibits quantum phase transitions similar to those observed in $B1$-type CeN. In Figs. 7(a) and 7(b), when lattice a is set at 2.50 Å, the momentum-resolved spectral function at 50 K does not indicate the presence of a Ce $-4f$ flat band near the Fermi level. Furthermore, the spectral density of Ce-$4f_{5/2}$ remains nearly unchanged between the low temperature of 50 K and the high temperature of 1000 K, suggesting a weak $c-f$ hybridization. However, when lattice a equals 3.029 Å, the spectral function at 50 K reveals that the Ce $-4f$ electrons have significantly shifted closer to the Fermi level when compared to the DFT result. Notably, a flat band feature emerges near the Fermi level, as shown in Fig. 7(c). The spectral density of Ce-$4f_{5/2}$ exhibits a sharp peak at the low temperature of 50 K, which diminishes significantly at the high temperature of 1000 K. This observation suggests strong electron renormalization effect, as shown in Fig. 7(d). When the lattice parameter is set to
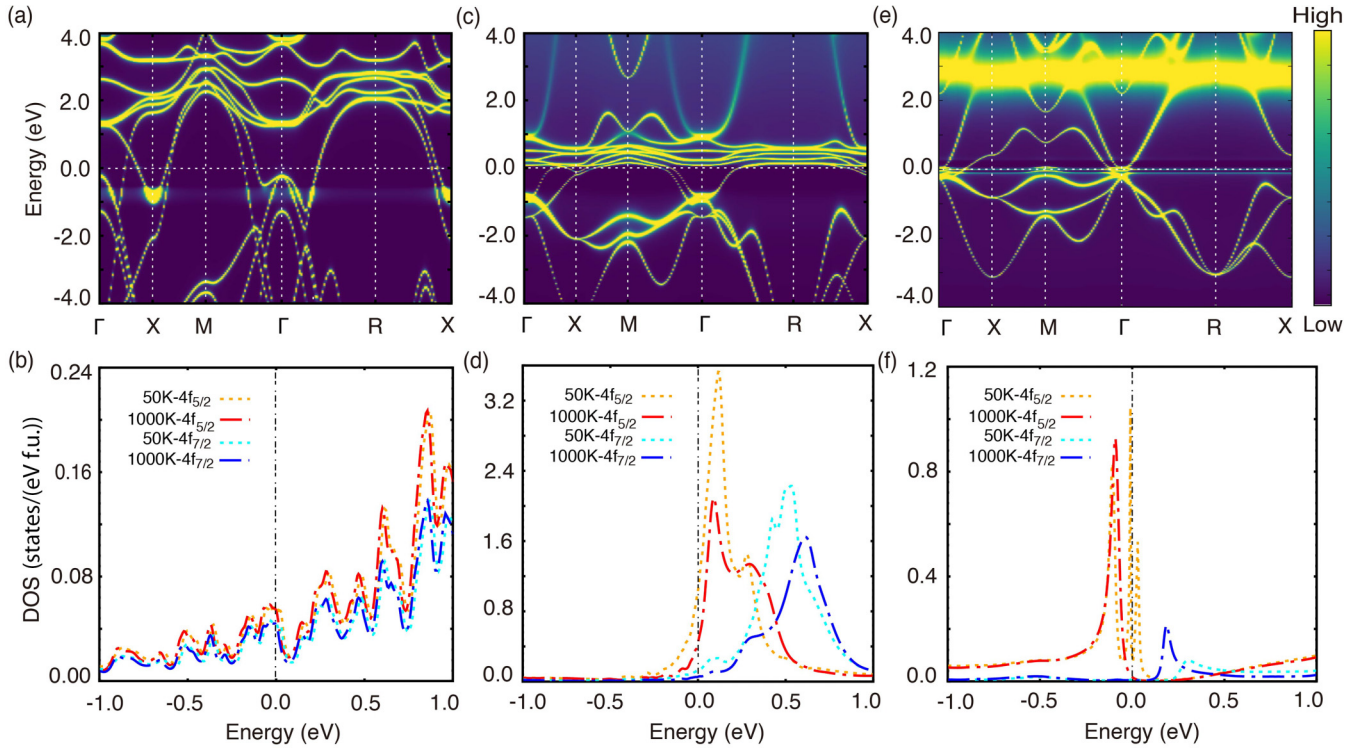
FIG. 7. The momentum-resolved spectral function and spectral density of $B2$-type CeN at different quantum states. [(a),(b)] In the mixed-valence state, the spectral function of CeN, when a equals 2.5 Å at 50 K. The spectral density of Ce-$4f_{5/2}$ and Ce-$4f_{7/2}$ at 50 and 1000 K. [(c),(d)] In the mixed-valence state, the spectral function of CeN, when a equals 3.029 Å at 50 K. The spectral density of Ce-$4f_{5/2}$ and Ce-$4f_{7/2}$ at 50 and 1000 K. [(e),(f)] In the Kondo metal state, the spectral function of CeN, when a equals 3.5 Å at 50 K. The spectral density of Ce-$4f_{5/2}$ and Ce-$4f_{7/2}$ at 50 and 1000 K.

3.5 Å, the Kondo behavior becomes even more pronounced. In Figs. 7(e) and 7(f), both the spectral function and spectral density of Ce-$4f_{5/2}$ demonstrate strong $c-f$ hybridization, with a notably sharper quasiparticle peak at 50 K. These results suggest that Ce $- 4f$ electrons display itinerant behavior at low temperatures and localized behavior at high temperatures.

To understand the quantum phase transitions in the $B2$ structure, we also study the number of occupied Ce $- 4f$ electrons n_f and the renormalization factor Z for Ce-$4f_{5/2}$ and Ce-$4f_{7/2}$ as a function of lattice parameter, as shown in the Fig. 8(a). For the $B2$ structure, there are only two phases. When the lattice a is less than 3.1 Å ($V/V_0 = 1.08$), the system is in a mixed-valence state. But the lattice a is in the range

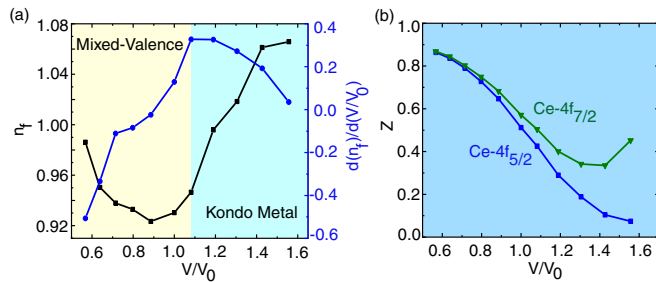

FIG. 8. The multi-quantum phase transitions. (a) The number of occupied $4f$ electrons n_f and derivative $d(n_f)/d(V/V_0)$. (b) The renormalization factor Z of Ce-$4f_{5/2}$ and Ce-$4f_{7/2}$ based on the volume of $B2$-type CeN at different compression and tension stresses.

3.1–3.5 Å ($V/V_0 = 1.08$–1.56), the system is in the Kondo-metal state. The conclusion is consistent with the derivative $d(n_f)/d(V/V_0)$, which presents the inflection point at a $=$ 3.1 Å. The renormalization factor Z for Ce-$4f_{5/2}$ and Ce-$4f_{7/2}$ is shown in Fig. 8(b). It shows that the renormalization factor Z of Ce-$4f_{5/2}$ is almost monotonic decrease along with the increase of lattice a, which means the Kondo behavior is obvious with a big lattice a. These results are in agreement with the analysis with $B1$ phase.

IV. CONCLUSIONS

CeN exhibits numerous anomalous properties, such as the lattice parameter of CeN is anomalously small compared with other rare-earth nitrides (Re-N) compounds. These anomalous physical properties of CeN are attributed to the distinctive behavior of the $4f$ electron in the Ce ion. CeN is regarded as a classic example of a mixed-valence compound. Under pressure, CeN presents two distinct phases, $B1$-type and $B2$-type. To investigate the behavior of the Ce $- 4f$ electrons, we employed the DFT+DMFT method to study the electronic structure of $B1$-type CeN, which is known to show mixed-valence behavior at ambient pressure. When we varied the temperature from 30 to 1000 K, it consistently exhibited mixed-valence behavior, with localized Ce $- 4f$ electrons displaying weak $c-f$ electron hybridization. This observation aligns with the results obtained from the analysis of the number of occupied $4f$ electrons n_f, the renormalization factor Z, and Fermi surface analyses. Furthermore, when we applied

global stress by compression and tension of $B1$-type CeN, we discovered that stress could induce multiple-quantum phase transitions. When the lattice a is smaller than 5.1 Å, the localized $Ce - 4f$ electrons present the mixed-valence state, having very weak $c-f$ electrons hybridization. But when a is among 5.1 and 5.6 Å, it shows very strong $c-f$ electrons hybridization near the Fermi level, forming Kondo metal, which can be supported from the spectral function, renormalization factor Z, Fermi surface and the imaginary part of real frequency self-energy analyses. Notably, when the lattice parameter extended beyond 5.6 Å, CeN exhibited insulating behavior. It means that $4f$ electrons have localization to iteration transition in CeN along with stress. Finally, we did the $B2$-type CeN electronic structure calculations by tuning stress, and observed similar behavior of the $4f$ electrons when compared to $B1$-type CeN. $B2$-type CeN also underwent a quantum phase transition, transitioning from a mixed-valence state to a Kondo metal state.

[1] Y.-f. Yang and D. Pines, Phys. Rev. Lett. **100**, 096404 (2008).

[2] J. Custers, K.-A. Lorenzer, M. Müller, A. Prokofiev, A. Sidorenko, H. Winkler, A. M. Strydom, Y. Shimura, T. Sakakibara, R. Yu *et al.*, Nat. Mater. **11**, 189 (2012).

[3] T. Park, F. Ronning, H. Q. Yuan, M. B. Salamon, R. Movshovich, J. L. Sarrao, and J. D. Thompson, Nature (London) **440**, 65 (2006).

[4] Y. Li, M. Liu, Z. Fu, X. Chen, F. Yang, and Y.-f. Yang, Phys. Rev. Lett. **120**, 217001 (2018).

[5] F. Hulliger, *Non-Metallic Compounds - II, Handbook on the Physics and Chemistry of Rare Earths* (Elsevier, Amsterdam, 1979), Vol. 4, pp. 153–236.

[6] H. R. Child, M. K. Wilkinson, J. W. Cable, W. C. Koehler, and E. O. Wollan, Phys. Rev. **131**, 922 (1963).

[7] N. Sclar, J. Appl. Phys. **35**, 1534 (1964).

[8] G. Busch, J. Appl. Phys. **38**, 1386 (1967).

[9] D. P. Schumacher and W. E. Wallace, J. Appl. Phys. **36**, 984 (1965).

[10] N. Sclar, J. Appl. Phys. **33**, 2999 (1962).

[11] S. Granville, C. Meyer, A. R. H. Preston, B. M. Ludbrook, B. J. Ruck, H. J. Trodahl, T. R. Paudel, and W. R. L. Lambrecht, Phys. Rev. B **79**, 054301 (2009).

[12] P. Larson, W. R. L. Lambrecht, A. Chantis, and M. van Schilfgaarde, Phys. Rev. B **75**, 045114 (2007).

[13] C. M. Aerts, P. Strange, M. Horne, W. M. Temmerman, Z. Szotek, and A. Svane, Phys. Rev. B **69**, 045115 (2004).

[14] D. L. Cortie, J. D. Brown, S. Brück, T. Saerbeck, J. P. Evans, H. Fritzsche, X. L. Wang, J. E. Downes, and F. Klose, Phys. Rev. B **89**, 064424 (2014).

[15] C. Li and D. Broido, Phys. Rev. B **95**, 205203 (2017).

[16] K. ODonnell and V. Dierolf, *Rare Earth Doped III-Nitrides for Optoelectronic and Spintronic Applications* (Springer, New York, 2014), Vol. 13.

[17] J. D. Miller, F. H. Ullstad, H. J. Trodahl, B. J. Ruck, and F. Natali, Nanotechnology **31**, 235202 (2020).

[18] S. Dhar, O. Brandt, M. Ramsteiner, V. F. Sapega, and K. H. Ploog, Phys. Rev. Lett. **94**, 037205 (2005).

[19] J. Q. Xiao and C. L. Chien, Phys. Rev. Lett. **76**, 1727 (1996).

[20] K. Senapati, M. Blamire, and Z. Barber, Nat. Mater. **10**, 849 (2011).

[21] M. N. Yoder, *Integrated Optics and Optoelectronics: A Critical Review*, edited by K. K. Wong and M. Razeghi (SPIE, Bellingham, WA, 1993), Vol. 10267, p. 102670F.

[22] H. Peng, C.-W. Lee, H. O. Everitt, C. Munasinghe, D. S. Lee, and A. J. Steckl, J. Appl. Phys. **102**, 073520 (2007).

[23] H. Imamura, Y. Sakata, T. Nuruyu, and T. Imahashi, J. Alloys Compd. **418**, 251 (2006).

[24] T. A. Yamamoto, T. Nakagawa, K. Sako, T. Arakawa, and H. Nitani, J. Alloys Compd. **376**, 17 (2004).

[25] T. Nakagawa, K. Sako, T. Arakawa, N. Tomioka, T. A. Yamamoto, K. Kamiya, and T. Numazawa, J. Alloys Compd. **408-412**, 187 (2006).

[26] L. Degiorgi, W. Bacsa, and P. Wachter, Phys. Rev. B **42**, 530 (1990).

[27] Y. Baer and C. Zürcher, Phys. Rev. Lett. **39**, 956 (1977).

[28] Y. Baer, R. Hauger, C. Zürcher, M. Campagna, and G. K. Wertheim, Phys. Rev. B **18**, 4433 (1978).

[29] G. L. Olcese, J. Phys. F: Met. Phys. **9**, 569 (1979).

[30] A. Schlegel, E. Kaldis, P. Wachter, and C. Zürcher, Phys. Lett. A **66**, 125 (1978).

[31] M. S. Litsarev, I. Di Marco, P. Thunström, and O. Eriksson, Phys. Rev. B **86**, 115116 (2012).

[32] A. Svane, Z. Szotek, W. M. Temmerman, J. L. gsgaard, and H. Winter, J. Phys.: Condens. Matter **10**, 5309 (1998).

[33] E. Wuilloud, B. Delley, W.-D. Schneider, and Y. Baer, J. Magn. Magn. Mater. **47-48**, 197 (1985).

[34] A. J. Freeman and G. H. Lander, *Handbook on the Physics and Chemistry of the Actinides* (Plenum, New York, 1985), Vol. 2.

[35] C. M. Varma, Rev. Mod. Phys. **48**, 219 (1976).

[36] A. Delin, P. M. Oppeneer, M. S. S. Brooks, T. Kraft, J. M. Wills, B. Johansson, and O. Eriksson, Phys. Rev. B **55**, R10173 (1997).

[37] V. Kanchana, G. Vaitheeswaran, X. Zhang, Y. Ma, A. Svane, and O. Eriksson, Phys. Rev. B **84**, 205135 (2011).

[38] S. Q. Xiao and O. Takai, Thin Solid Films **317**, 137 (1998).

[39] T.-Y. Lee, D. Gall, C.-S. Shin, N. Hellgren, I. Petrov, and J. E. Greene, J. Appl. Phys. **94**, 921 (2003).

[40] J. S. Olsen, J.-E. Jørgensen, L. Gerward, G. Vaitheeswaran, V. Kanchana, and A. Svane, J. Alloys Compd. **533**, 29 (2012).

[41] J. P. Perdew, K. Burke, and M. Ernzerhof, Phys. Rev. Lett. **77**, 3865 (1996).

[42] P. Blaha, K. Schwarz, G. K. H. Madsen, D. Kvasnicka, and J. Luitz, *WIEN2k, An Augmented Plane Wave Plus Local Orbitals Program for Calculating Crystal Properties* (Vienna University of Technology, Austria, 2001).

[43] G. Kresse and J. Furthmüller, Comput. Mater. Sci. **6**, 15 (1996).

[44] G. Kresse and J. Furthmüller, Phys. Rev. B **54**, 11169 (1996).

[45] P. E. Blöchl, Phys. Rev. B **50**, 17953 (1994).

[46] G. Kotliar, S. Y. Savrasov, K. Haule, V. S. Oudovenko, O. Parcollet, and C. A. Marianetti, Rev. Mod. Phys. **78**, 865 (2006).

[47] E. Gull, A. J. Millis, A. I. Lichtenstein, A. N. Rubtsov, M. Troyer, and P. Werner, Rev. Mod. Phys. **83**, 349 (2011).

[48] K. Haule, Phys. Rev. Lett. **115**, 196403 (2015).

[49] D.-C. Ryu, J. Kim, K. Kim, C.-J. Kang, J. D. Denlinger, and B. I. Min, Phys. Rev. Res. **2**, 012069(R) (2020).

[50] K. Haule, C.-H. Yee, and K. Kim, Phys. Rev. B **81**, 195107 (2010).

[51] M. Jarrell and J. E. Gubernatis, Phys. Rep. **269**, 133 (1996).

[52] A. W. Lawson and T.-Y. Tang, Phys. Rev. **76**, 301 (1949).

[53] See Supplemental Material at http://link.aps.org/supplemental/10.1103/PhysRevB.109.125114 for the details of DFT band structure and DOS of B1-type CeN, without and with SOC effect.

[54] O. Bodensiek, R. Žitko, M. Vojta, M. Jarrell, and T. Pruschke, Phys. Rev. Lett. **110**, 146406 (2013).